



# Quark matter in strong magnetic fields

Débora Peres Menezes

Universidade Federal de Santa Catarina, Departamento de Física–CFM–CP 476, Campus  
Universitário–Trindade, CEP 88040-900, Florianópolis–SC, Brazil

**Abstract.** In the present work we are interested in understanding various properties of quark matter described by the Nambu-Jona-Lasinio (NJL) model once it is subject to strong magnetic fields. We start by analysing the possible different phase diagram structures. Secondly, we investigate the differences arising from different vector interactions in the Lagrangian densities and apply the results to stellar matter. We then look at deconfinement and chiral restoration properties at zero chemical potential with the (entangled) Polyakov NJL models. Finally, we investigate the position of the critical end point for different chemical potential and density scenarios.

## 1 Motivation and Results

The study of the QCD phase diagram, when matter is subject to strong external magnetic fields has been a topic of intense investigation recently. The fact that magnetic fields can reach intensities of the order of  $B \sim 10^{19}$  G or higher in heavy-ion collisions [1] and up to  $10^{18}$  G in the center of magnetars [2] made theoretical physicists consider matter subject to magnetic field both at high temperatures and low densities and low temperatures and high densities. We describe quark matter subject to strong magnetic fields within the SU(3) (E)PNJL model with vector interaction:

$$\begin{aligned} \mathcal{L} = & \bar{\psi}_f [i\gamma_\mu D^\mu - \hat{m}_f] \psi_f + \mathcal{L}_{\text{sym}} + \mathcal{L}_{\text{det}} \\ & + \mathcal{L}_{\text{vec}} + \mathcal{U}(\Phi, \bar{\Phi}; T) - \frac{1}{4} F_{\mu\nu} F^{\mu\nu}, \end{aligned} \quad (1)$$

with

$$\begin{aligned} \mathcal{L}_{\text{sym}} = & G \sum_{a=0}^8 [(\bar{\psi}_f \lambda_a \psi_f)^2 + (\bar{\psi}_f i\gamma_5 \lambda_a \psi_f)^2], \\ \mathcal{L}_{\text{det}} = & -K \{ \det_f [\bar{\psi}_f (1 + \gamma_5) \psi_f] + \det_f [\bar{\psi}_f (1 - \gamma_5) \psi_f] \}, \end{aligned}$$

where  $\psi_f = (u, d, s)^T$  represents a quark field with three flavors,

$$\hat{m}_c = \text{diag}_f(m_u, m_d, m_s)$$

is the corresponding (current) mass matrix,  $\lambda_0 = \sqrt{2/3}I$  where  $I$  is the unit matrix in the three flavor space, and  $0 < \lambda_a \leq 8$  denote the Gell-Mann matrices. The

coupling between the magnetic field  $B$  and quarks, and between the effective gluon field and quarks is implemented *via* the covariant derivative  $D^\mu = \partial^\mu - iq_f A_{EM}^\mu - iA^\mu$  where  $q_f$  represents the quark electric charge,  $A_\mu^{EM} = \delta_{\mu 2} \times_1 B$  is a static and constant magnetic field in the  $z$  direction and  $F_{\mu\nu} = \partial_\mu A_\nu^{EM} - \partial_\nu A_\mu^{EM}$ . To describe the pure gauge sector an effective potential  $\mathcal{U}(\Phi, \bar{\Phi}; T)$  is chosen:

$$\frac{\mathcal{U}(\Phi, \bar{\Phi}; T)}{T^4} = -\frac{a(T)}{2} \bar{\Phi} \Phi + b(T) \ln [1 - 6\bar{\Phi} \Phi + 4(\bar{\Phi}^3 + \Phi^3) - 3(\bar{\Phi} \Phi)^2],$$

where  $a(T) = a_0 + a_1 \left(\frac{T_0}{T}\right) + a_2 \left(\frac{T_0}{T}\right)^2$ ,  $b(T) = b_3 \left(\frac{T_0}{T}\right)^3$ . The standard choice of the parameters for the effective potential  $\mathcal{U}$  is  $a_0 = 3.51$ ,  $a_1 = -2.47$ ,  $a_2 = 15.2$ , and  $b_3 = -1.75$ . Besides the PNJL model, where  $G$  denotes the coupling constant of the scalar-type four-quark interaction in the NJL sector, we consider an effective vertex depending on the Polyakov loop ( $G(\Phi, \bar{\Phi})$ ): the EPNJL model. This effective vertex

$$G(\Phi, \bar{\Phi}) = G [1 - \alpha_1 \Phi \bar{\Phi} - \alpha_2 (\Phi^3 + \bar{\Phi}^3)]. \quad (2)$$

generates entanglement interactions between the Polyakov loop and the chiral condensate.

As for the vector interaction, the Lagrangian density that denotes the  $U(3)_V \otimes U(3)_A$  invariant interaction is

$$\mathcal{L}_{vec} = -G_V \sum_{a=0}^8 [(\bar{\psi} \gamma^\mu \lambda_a \psi)^2 + (\bar{\psi} \gamma^\mu \gamma_5 \lambda_a \psi)^2]. \quad (3)$$

and a reduced NJLv Lagrangian density can be written as

$$\mathcal{L}_{vec} = -G_V (\bar{\psi} \gamma^\mu \psi)^2. \quad (4)$$

In the  $SU(3)$  NJLv model, the above Lagrangian densities are not identical in a mean field approach and we discuss both cases next. We refer to the Lagrangian density given in Eq. (3) as model 1 (P1) and to the Lagrangian density given in Eq. (4) as model 2 (P2).

Our first task was to analyse the possible different phase diagram structures at zero temperature. We have seen that the number of intermediate phases depends on the number of *jumps* appearing in the dressed quark masses, which in turn, depend on the number of filled Landau levels. The chiral susceptibilities, as usually defined, are different not only for the  $s$ -quark as compared with the two light quarks, but also for the  $u$  and  $d$ -quarks, yielding non identical crossover lines for the light quark sector. A typical diagram is shown in Figure 1 and details are given in Ref. [3]. Next, the effect of the vector interaction on three flavor magnetized matter was studied for cold matter within two different models usually found in the literature, a flavor dependent (P1) [4] and a flavor independent one (P2) [5]. We have seen that the flavor independent vector interaction predicts a smaller strangeness content and, therefore, harder equations of state. On the other hand, the flavor dependent vector interaction favors larger strangeness content the larger the vector coupling, as can be seen in Figure 2. At low densities

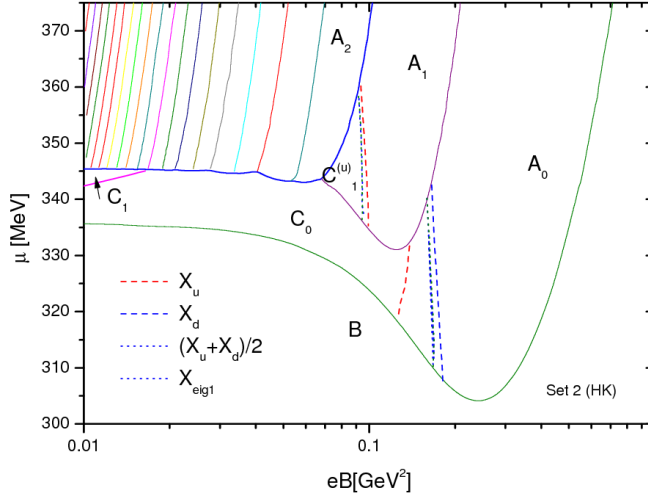


**Fig. 1.** Phase diagrams in the  $eB - \mu$  plane.

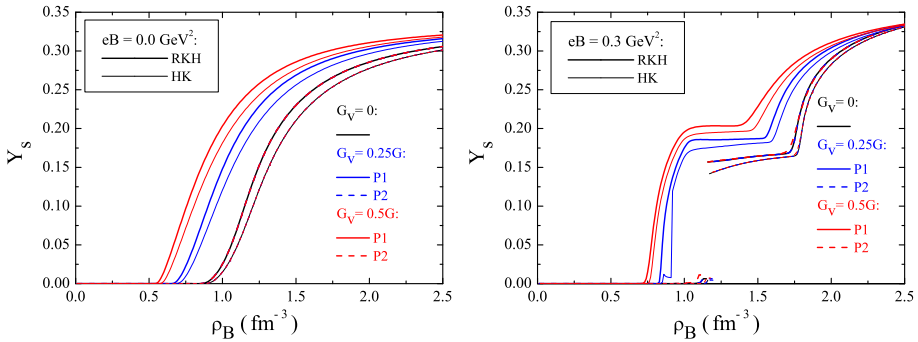


**Fig. 2.** The strangeness fraction as a function of the baryonic density for models P1 and P2 and different values of  $G_V$ , and a)  $B = 0$ ; b)  $eB = 0.3 \text{ GeV}^2$ .

the magnetic field and the vector interaction have opposite competing effects: the first one softens the equation of state while the second hardens it. Quark stars and hybrid stars subject to an external magnetic field were also studied. Larger star masses are obtained for the flavor independent vector interaction and maximum masses of the order of  $2 M_\odot$  can be achieved depending on the value of the vector interaction and on the intensity of the magnetic field. Hybrid stars may bare a core containing deconfined quarks if neither the vector interaction nor the magnetic field are too strong. Also, the presence of strong magnetic fields seems to disfavor the existence of a quark core in hybrid stars. Mass radius curves for quark and hybrid stars can be seen in Figure 3. Details and quantitative results are given in Ref. [6].

Then, we move to finite temperature and study the behavior of the quark condensates at zero chemical potential within three flavor PNJL and EPNJL models. We have shown that the chiral and deconfinement transition temperatures

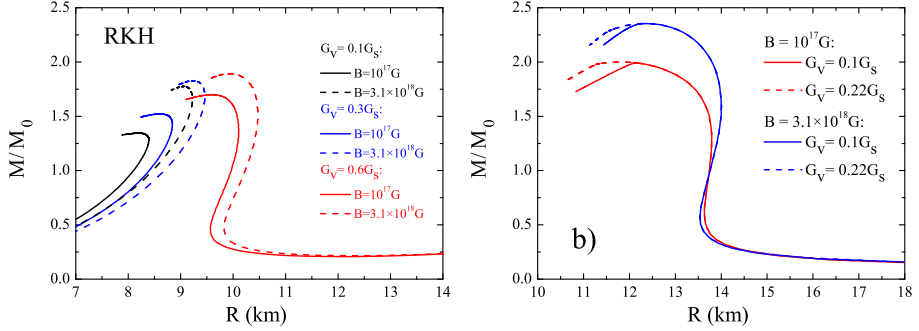


**Fig. 3.** Mass radius curves obtained with P2 for different values of  $G_V$ , two intensities of the magnetic field, parametrization RKH for a) quark and b) hybrid stars.

increase in the presence of an external magnetic field and that, at  $T = 0$  the quantitative behaviors of SU(3) PNJL and EPNJL are closer to the lattice results. The effect of the magnetic field on the EPNJL deconfinement and chiral transition temperatures is such that the existing coincidence at  $eB = 0$  is destroyed by the magnetic field. For finite temperatures, the inverse magnetic catalysis found in lattice calculations can be obtained if the the magnetic field back-reaction on the Polyakov loop is taken into account by a magnetic field dependent scale parameter  $T_0$ . Details about these results are given in Ref. [7].

Finally, the location of the critical end point (CEP) on the QCD phase diagram was calculated within different scenarios with respect to the isospin and strangeness content of matter, as shown in Figure 4 left for non-magnetized matter. It was shown that for  $\beta$ -equilibrium matter the CEP occurs at smaller temperatures and densities. This scenario is of interest for neutron stars and confirms previous calculations that indicate that a deconfinement phase transition in the laboratory will be more easily attained with asymmetric nuclear matter. A more interesting situation was observed when analyzing very isospin asymmetric matter subject to different intensities of the magnetic field, as seen in Figure 4 right. Starting from a scenario having an isospin asymmetry above which the CEP does not exist for a zero external magnetic field it was shown that a sufficiently high external magnetic field could drive the system to a first order phase transition. The critical end point occurs at very small temperatures if  $eB < 0.1 \text{ GeV}^2$  and, in this case, a complicated structure with several CEP at different values of  $(T, \mu_B)$  are possible for the same magnetic field, because the temperature is not high enough to wash out the Landau level effects. For  $eB > 0.1 \text{ GeV}^2$  only one CEP exists. This is an important result because it shows that a strong magnetic field is able to drive a system with no CEP into a first order phase transition. More details are given in Ref. [8].

**Acknowledgements.** The co-authors of different parts of this work are Constança Providência, Marcus Benghi Pinto, Norberto Scoccola, Luis R. B de Castro, Pedro Costa, Márcio Ferreira and Ana G. Grunfeld and this work was partially

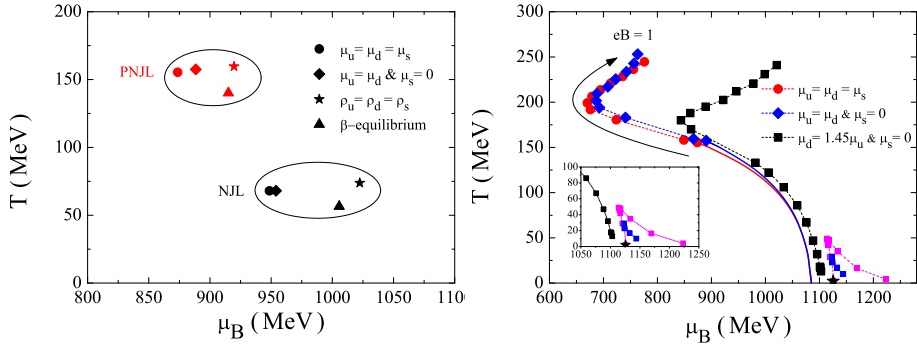


**Fig. 4.** Left - Location of the CEP on a diagram  $T$  vs the baryonic chemical potential under different scenarios and models (NJL, PNJL). No external magnetic field is considered. Right - Effect of an external magnetic field on the CEP location within PNJL model for three different scenarios.

supported by CNPq (Brazil), CAPES (Brazil) and FAPESC (Brazil) under project 2716/2012,TR 2012000344.

## References

1. K. Fukushima, D. E. Kharzeev and H. J. Warringa, *Phys. Rev. D* **78** (2008) 074033; D. E. Kharzeev and H. J. Warringa, *Phys. Rev. D* **80** (2009) 034028.
2. R. Duncan and C. Thompson, *Astrophysical Journal, Part 2 – Letters* **392** (1992) L9–L13; C. Kouveliotou et al, *Nature* **393** (1998) 235.
3. Ana G. Grunfeld, Debora P. Menezes, Marcus B. Pinto and Norberto Scoccola, *Phys. Rev. D* (2014) in press, [arXiv:1402.4731v1](https://arxiv.org/abs/1402.4731v1) [hep-ph].
4. S. Klimt, M. Lutz, and W. Weise, *Phys. Lett. B* **249** (1990) 386; M. Hanauske, L. M. Satarov, I. N. Mishustin, H. Stöcker and W. Greiner, *Phys. Rev. D* **64** (2001) 043005.
5. K. Fukushima, *Phys. Rev. D* **78** (2008) 114019.
6. Debora P. Menezes, Marcus B. Pinto, Luis R. B de Castro, Constança Providencia and Pedro Costa, *Phys. Rev. C* **89** (2014) 055207.
7. M. Ferreira, P. Costa, D.P. Menezes, C. Providencia and N. Scoccola, *Phys. Rev. D* **89** (2014) 016002.
8. Pedro Costa, Márcio Ferreira, Hubert Hansen, Débora P. Menezes, Constança Providência, *Phys. Rev. D* **89** (2014) 056013.

## Kvarkovski propagator v coulombski umeritvi kvantne kromodinamike

Y. Delgado<sup>a</sup>, M. Pak<sup>a</sup>, M. Schröck<sup>b</sup>

<sup>a</sup> Institut für Physik, Karl-Franzenz Universität Graz, 8010 Graz, Austria

<sup>b</sup> Istituto Nazionale di Fisica Nucleare (INFN), Sezione di Roma Tre, Rome, Italy

Proučujemo kvarkovski propagator na konfiguracijah gašenega umeritvenega polja v coulombski umeritvi. Pri tem uporabimo kiralno simetrične "prekrivalne fermione". V tej umeritvi lahko povežemo "funkcijo oblačenja" kvarkovskega propagatorja s priporom in kiralno simetrijo kromodinamike. Pripor lahko pripišemo infrardeče divergentni vektorski "funkciji oblačenja". Izvrednotimo "funkcije oblačenja" kvarkovskega propagatorja, razberemo dinamično maso kvarka in ekstrapoliramo vse te količine proti kiralni limiti. Končno razpravljamo, kako se odstranijo nizke Diracove ekscitacije.

## Mase oblečenih kvarkov in barionska spektroskopija

W. Plessas

Theoretical Physics, Institute of Physics, University of Graz, A-8010 Graz, Austria

Prikažemo hierarhijo mas oblečenih kvarkov, ki prevladujejo v efektivnih modelih kvantne kromodinamike, zlasti v relativističnem modelu z oblečenimi kvarki. Opazimo, da je presežek dinamično generirane mase nad golo maso bolj ali manj neodvisen od okusa kvarkov in znaša  $\Delta m \approx (370 \pm 30)$  MeV. Podobne vrednosti dajo tudi alternativni efektivni opisi barionske spektroskopije, na primer Dyson-Schwingerjev pristop.

## Primerjava jedrskih potencialov za hiperon Lambda in za nukleon

Bogdan Povh<sup>a</sup> in Mitja Rosina<sup>b,c</sup>

<sup>a</sup> Max-Planck-Institut für Kernphysik, Postfach 103980, D-69029 Heidelberg, Germany

<sup>b</sup> Fakulteta za matematiko in fiziko, Univerza v Ljubljani, Jadranska 19, p.p.2964, 1001 Ljubljana, Slovenija

<sup>c</sup> Institut J. Stefan, 1000 Ljubljana, Slovenija

Raziskujemo verjetni mehanizem, zakaj čuti hiperon  $\Lambda$  dvakrat šibkejše jedrsko polje (okrog  $-27$  MeV) kot nukleon (okrog  $-50$  MeV).